X-ray analysis of protective coatings

Zoestbergen, Edzo

5 Stress state of TiN/TiAlN multi-layers

Physical vapour deposition, PVD, enables the production of coatings composed of multi-layers, which may combine the advantages of the separate components into a single coating. The TiN/TiAlN multi-layer system [1,2] is an example of this and combines the higher oxidation resistance, hardness and abrasive resistance of TiAlN [3,4] at higher temperatures with the superior performance of TiN at lower temperatures.

In this chapter a study is presented of the microstructure, morphology and the state of stress of TiN and TiN/TiAlN coatings. The refractory hard coatings, TiN and a multi-layer system of TiN/TiAlN, were deposited by means of PVD by Balzers using a standard commercial process. The layers are deposited onto two different substrates; stainless steel AISI 304 and tool steel AISI D2.

The exact microstructure of the coatings was determined with a Philips FEG-XL30 scanning electron microscope and the composition of the coatings was investigated with energy dispersive X-ray spectroscopy (EDS) and Auger electron spectroscopy (AES) [5]. The residual stresses were determined using X-ray diffraction.

5.1 Structure and chemical composition

To study the microstructure of the multi-layer system cross sections of the coatings were prepared. Figure 5.1 shows an SEM image of a polished cross section of a TiN/TiAlN multi-layer on stainless steel. The difference in contrast between the multi-layers is due to a difference in composition and the amount of Al being higher in the darker areas than in the lighter ones. The thickness of the multi-layers is approximately 150 nm. The change in contrast at the top of the coating is caused by the preparation method, i.e. the polishing rounds off the top of the coating and this influences the brightness and so it is difficult to determine the microstructure right at the top. The multi-layer coating on tool steel shows the same structure as the multi-layers on stainless steel.

The micrograph in Figure 5.2 is obtained by breaking a coated tool steel specimen after cooling in liquid nitrogen. There are different layers visible within the lighter layers. In total there are four light and three dark layers visible with approximately the same thickness, 15-20 nm.

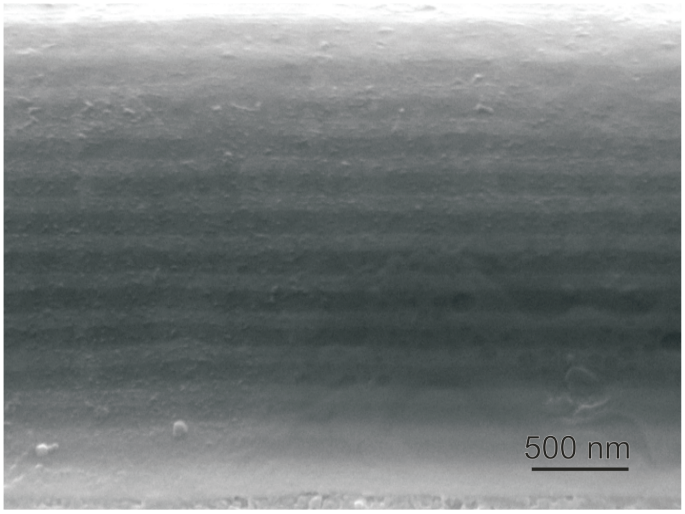

Figure 5.1 Cross sectional micrograph of TiN/TiAlN on stainless steel. The difference in colour is related to the difference in composition.

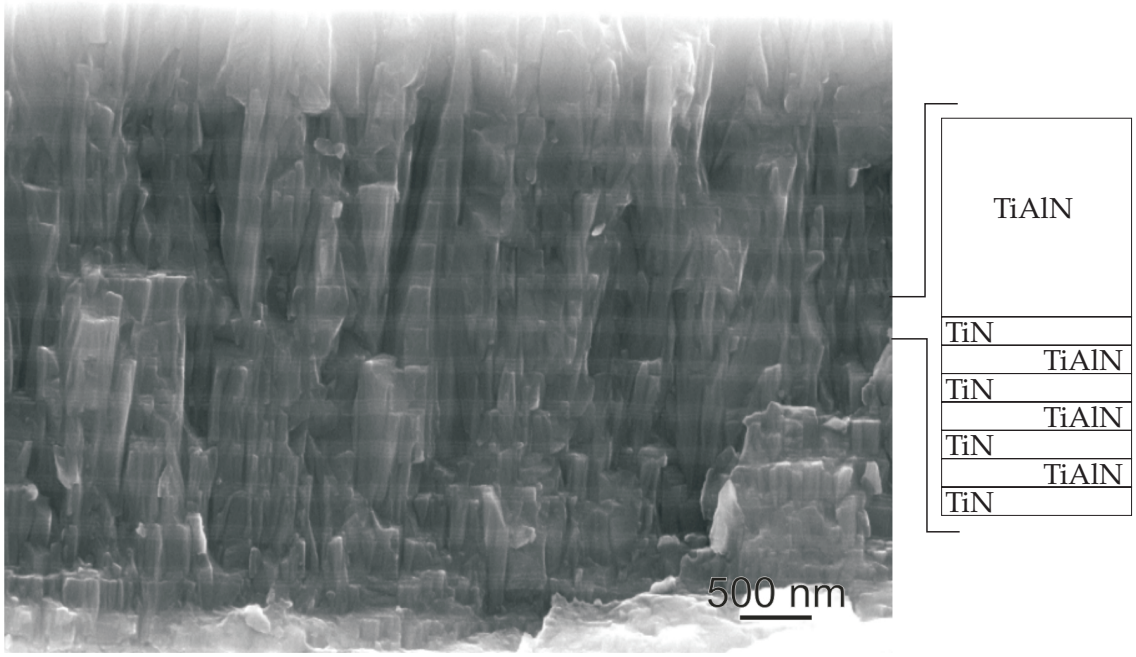

Figure 5.2 Cross sectional micrograph of TiN/TiAlN on tool steel. Within the lighter areas there are also dark lines visible.

With a dedicated local-probe UHV scanning Auger microscope, with a lateral resolution of about 15 nm derived from a JAMP7800 FEG, a depth profile of the coating is made. The coating is removed by sputtering with Ar ions during intervals of one minute. In between the sputter cycles the Ti and Al concentrations are measured. This process is continued until the complete coating is removed. The normalised intensities, i.e. the intensity of one element divided by the sum of the intensities of the two elements, are plotted in Figure 5.3 as a function of the sputter time. After 222 minutes the entire coating is removed. This is visible in the large scattering of the graphs due to the normalisation of the intensities. The value of 222 minutes can be used to determine the thickness of the layer, which is removed during each cycle, i.e. 20 [nm][cycle^{-1}].

In the first part there is a relatively higher concentration of Al so it appears that the first layer is a TiAlN layer with a thickness of ≈400 nm. After this the Ti and Al concentrations vary and when the Ti concentration is high the Al concentration is low and vice versa. It is not possible to measure within the smaller set of sub-layers. There are three reasons for this:

- Firstly, the sub-layers have a thickness, which is comparable to the thickness of the layer removed during each cycle.
- Secondly, preferential sputtering during the layer removal can generate a surface roughness.
- Finally due to ion beam mixing the atoms of a layer may be implanted into other sub-layers.

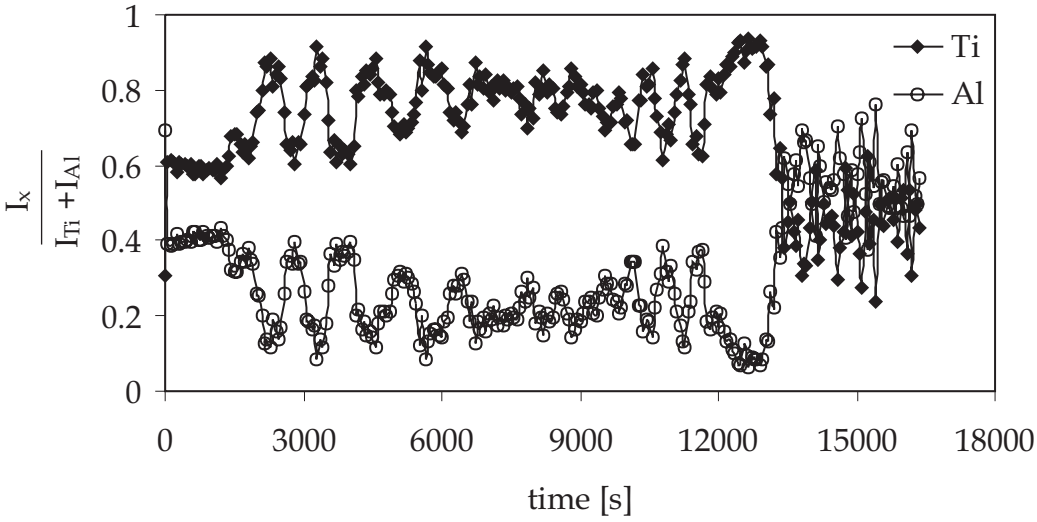

Figure 5.3 Normalised intensity of Ti and Al measured with the SAM.

Near the interface with the substrate there is an area of 400 nm where the Ti concentration is significantly higher than the Al concentration.

With EDS the atomic ratio of Al versus Ti is measured. The EDS results show that the ratio changes with the position. At the top of the coating, the atomic percentages are 37.59 atom% Al and 62.41 atom% Ti, in the middle 32.72 atom% Al and 67.28 atom% Ti and near the interface with the substrate 8.83 atom% Al and 91.17 atom% Ti. This is in agreement with the idea that on top there is a thicker $Ti_xAl_{1-x}N$ layer and at the interface with the substrate there is a thicker TiN interlayer present. The TiN interlayer is used to improve the adhesion between the coating and the substrate [2]. Between these layers the ratio of Al to Ti is 1:2, confirming that the chemical composition and structure is not TiAlN/TiN but TiAlN/(TiN/TiAlN), as otherwise the ratio Ti:Al would be 3:1.

5.2 Crystallographic orientation

The crystallographic phases and chemical compositions of the substrates are investigated with X-rays. The diffraction intensities of stainless steel and tool steel are shown in Figure 5.4. The stainless steel consists mainly of α and γ Fe, Ni-Fe-Cr, and the tool steel constitutes of α-Fe and a chromium carbide, Cr_7C_3.

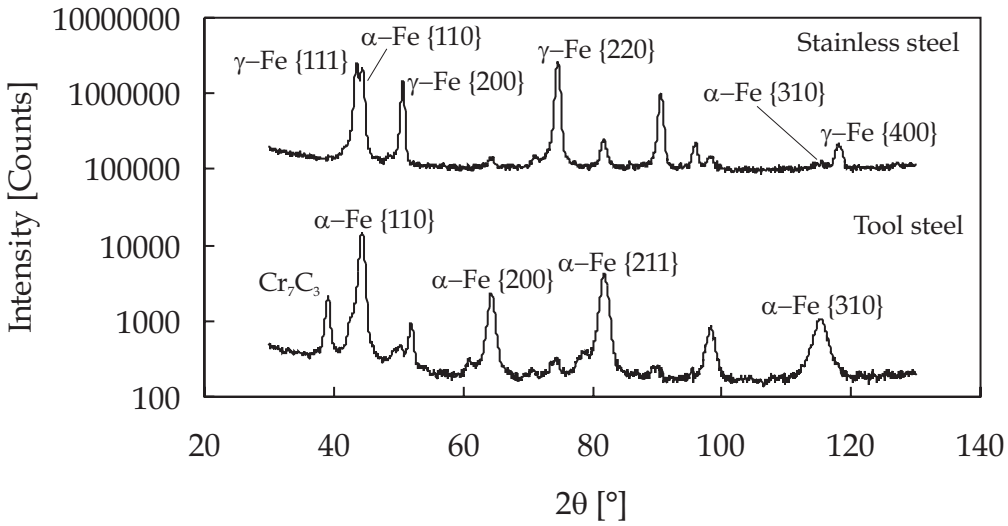

Figure 5.4 Diffraction patterns of uncoated substrates. The top one is of stainless steel and the bottom one is of tool steel.

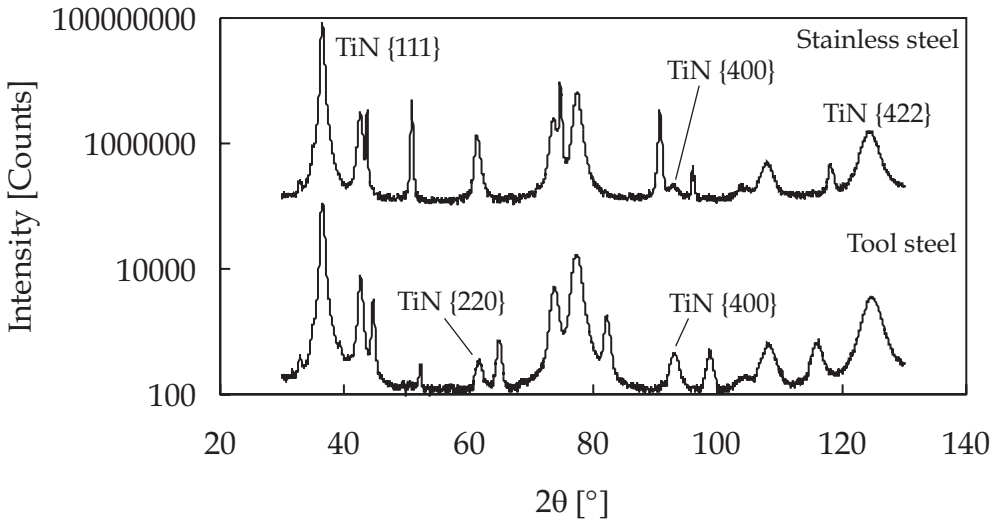

Figure 5.5 Substrates coated with TiN.

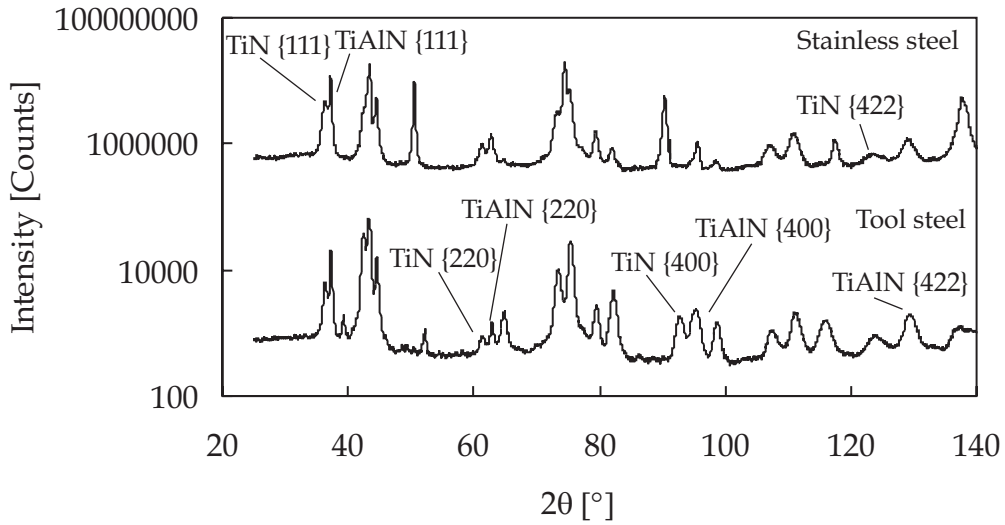

Figure 5.6 Substrates coated with TiN/TiAlN.

Figures 5.5 and 5.6 show the diffraction patterns of the coated stainless steel and tool steel. The substrates coated with the multi-layer systems have, besides the TiN peaks, also a peak due to the TiAlN layers with a lattice spacing somewhat smaller than TiN, ≈4.18Å [2,3,6]. This rather small difference in lattice spacing makes it impossible to carry out accurate texture measurements on the multi-layer systems. However, it is possible to use the integrated intensities of the different reflections of Figures 5.5 and 5.6 to draw some conclusions about the crystallographic orientation of the coatings. In order to perform an appropriate comparison of the integrated peak intensities it is necessary to correct the data with intensities from a random powder diffraction pattern of the same material.

In this case a correction for the finite coating thickness which will introduce a 2θ dependency must also be taken into account. This results in:

$$I_{\{hkl\}}^{comparison} = \frac{I_{\{hkl\}}}{I_{\{hkl\}powder}} \cdot \frac{\sin\theta_{\{hkl\}}}{\int_0^d e^{-\frac{2\mu \cdot z}{\sin\theta_{\{hkl\}}}} dz} \tag{5.1}$$

Here $I_{\{hkl\}}$ is the relative intensity of the {hkl} planes of the coating, $I_{\{hkl\}\ powder}$ is the relative intensity of the {hkl} planes of a randomly oriented polycrystalline powder, μ is the linear absorption coefficient of the coating and θ is the Bragg angle of a particular set of planes. The $I_{\{hkl\}\ powder}$ for TiN is assumed to be the same as the JCPDS powder diffraction files. For TiAlN the relative intensities are calculated assuming that the space group is Fm3m with a stoichiometry of $Ti_{0.5}Al_{0.5}N$ and a random distribution of titanium and aluminium atoms, see Table 5.1 [7].

Table 5.1 Relative intensities [%]. Data for TiN are from JCPDS powder diffraction files and the values of TiAlN are calculated.

Material	TiAlN	TiN
{111}	51	72
{200}	100	100
{220}	50	45
{311}	17	19
{222}	14	12
{400}	6	5
{331}	7	6
{420}	19	14
{422}	20	12

Data for the corrected intensities of the TiN films are presented in Table 5.2. The results show that the {111} diffraction has the highest intensity, which is in agreement with the most common texture in TiN PVD coatings, namely the characteristic {111} fibre texture. This {111} texture is visible for both the TiN coating on stainless steel and on tool steel. However, there is one remarkable feature, the intensities of the {111} and {222} reflections are approximately the same for the TiN on stainless steel but not for TiN on tool steel. The same feature is present in the intensities of the {200} and {400} reflections. In the coating on tool steel the intensity of the {400} reflections is higher than that of the {200} reflections. The reason for this is not yet clear.

Table 5.2 Corrected integrated α_1 intensities of the reflections of the TiN layers on stainless and on tool steel [counts].

Substrate	Stainless steel	Tool steel
{111}	11920	13270
{200}	-	730
{220}	570	100
{311}	3600	5360
{222}	16210	37330
{400}	250	2020
{331}	560	450
{420]	1545	1750
{422}	9660	17106

Table 5.3 lists the corrected α_1 intensities of the multi-layer systems. It is clearly visible that the intensities of the TiAlN peaks are higher than the TiN peaks. Inspecting the intensities it is clear that the {111} planes have not the highest intensity, as can also be seen from Figure 5.6. The reflection with the highest intensity is the {311} reflection and this is the case for the layers on both substrates. This is confirmed by intensity measurements, which were performed on the {422} reflections. In the case of a {311} fibre texture the {422} reflections must have a maximum intensity at three ψ angles lying at: 10°, 42.4°, and 60.5° in the range from 0 to 70° ψ. In Figure 5.7 the intensity of the {422} reflections of TiAlN is plotted as a function of the ψ angle and there are indeed

Table 5.3 Corrected integrated α_1 intensities of the reflections of the TiN and the TiAlN from the multi-layers on stainless and on tool steel [counts].

Substrate	Stainless steel		Tool steel	
System	TiN	TiAlN	TiN	TiAlN
{111}	1000	1450	700	1900
{200}	-	-	-	-
{220}	290	360	150	200
{311}	4720	7160	8000	21390
{222}	-	1540	-	2070
{400}	-	-	7320	9890
{331}	-	-	-	-
{420}	-	2470	-	2900
{422}	1975	1930	2540	3150

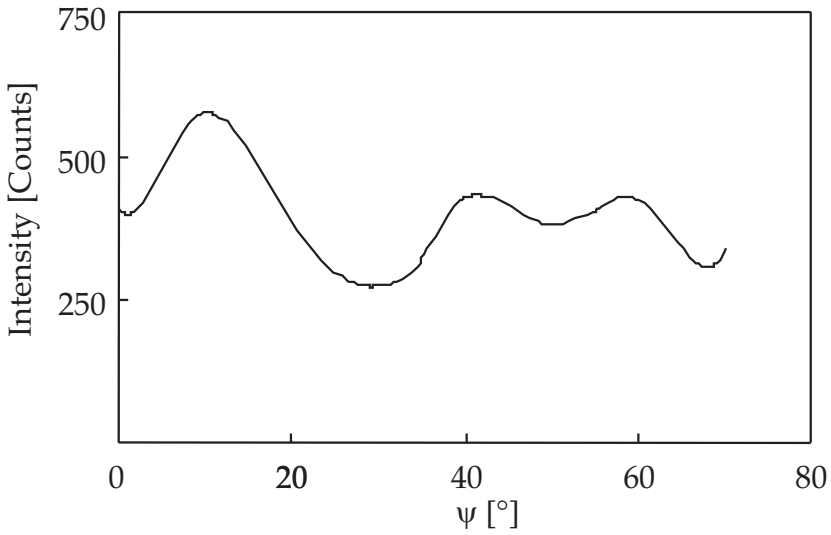

Figure 5.7 Peak intensity of the {422} planes as a function of the ψ angle. There are three maxima visible.

three local maxima at the correct ψ angles.

The {311} texture is in contrast with results from literature, reporting that the main texture in TiAlN layers is a {200} fibre texture or in some cases a {111} texture [3,8,9]. Looking at the intensities of the {200} and {400} peaks, there are no {200} and {400} peaks visible for the coating on the stainless steel substrate. This is different for the coating on tool steel. Here there are distinct {200} and {400} peaks visible for both the TiN and TiAlN sub-layers. Therefore, the texture in both systems is a {311} texture, but there is a difference between coatings deposited on different substrates.

5.3 Residual stresses

To be able to calculate the residual stresses in the coating it is necessary to determine the strain in the specimens. This is done by measuring the lattice spacing of a particular plane as a function of its orientation. For the multi-layer systems there is an additional problem and that is that the lattice spacing of the TiN and the TiAlN are almost identical. For the lower indices planes this puts a restriction on the ψ range for which the lattice spacing can be determined and therefore the {422} planes are used for the strain measurements. In Figure 5.8 the lattice spacing of the multi-layer on stainless steel is plotted versus the d-$\sin^2\psi$. Both the TiAlN and the TiN sub-layers show a linear relation between the

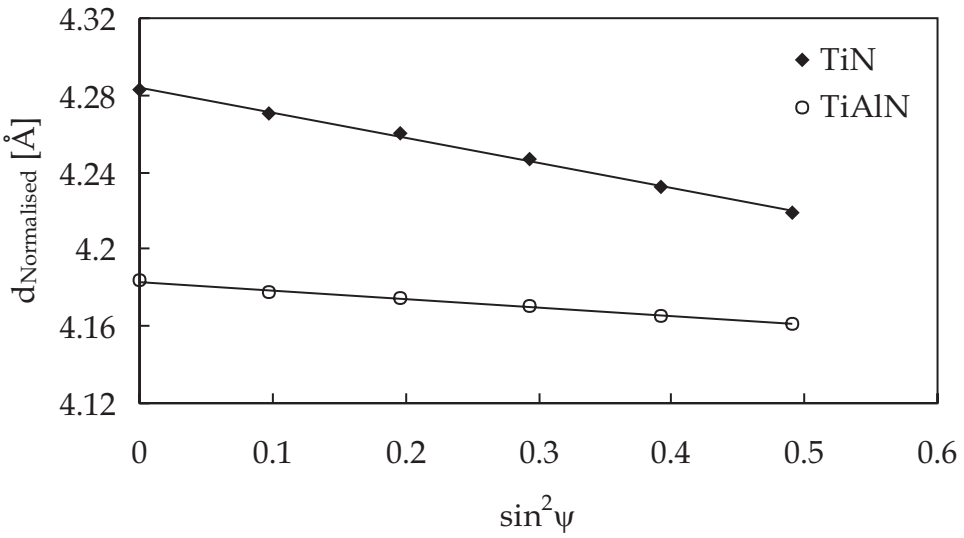

Figure 5.8 Normalised lattice spacings for TiN/TiAlN on stainless steel. For both materials there is a linear relation between the lattice spacing and the $\sin^2\psi$.

lattice spacing and the $\sin^2\psi$. Therefore, the use of linear isotropic elasticity seems to be permitted [10].

Using Equation (3.7) and knowing the mechanical XEC makes it possible to calculate the residual stresses. The Young's modulus for TiAlN is approximately the same as for TiN [1], and from the measurements on the different specimens it is possible to determine the Poisson's ratio. When the state of stress is biaxial and axial symmetrical, the ψ value for which $d_{\varphi\psi}$ is equal to d_0 is given by:

$$\sin^2\psi = \frac{2\nu}{1+\nu} \tag{5.2}$$

This value is independent on the level of residual stress and depends solely on the Poisson's ratio. Plotting for different specimens the value of the d-$\sin^2\psi$ graph at $\sin^2\psi$=0 versus the slope, G_s, of the d-$\sin^2\psi$ graph will result in a new graph. In this graph the intercept at G_s=0 is the d_0 and the slope of this curve is the $\sin^2\psi$ value for which $d_{\varphi\psi}=d_0$ [11]. One should realise that the accuracy in the slope is larger than in the intercept as the d_0 is found by extrapolating the $\sin^2\psi$ to zero. For the TiN there are four points available, the pure TiN layers and the TiN sub-layer in the TiN/TiAlN multi-layer systems. Both systems were deposited onto stainless steel and tool steel. For the TiAlN there are only two points available and this will influence the accuracy of the values obtained. The results are presented in Figure 5.9 and Table 5.4. The relation between the

intercepts and the slopes of the TiN is clearly linear and the calculated Poisson's ratio is in agreement with values from literature [12]. The Poisson's ratio of the TiAlN is smaller than that of TiN.

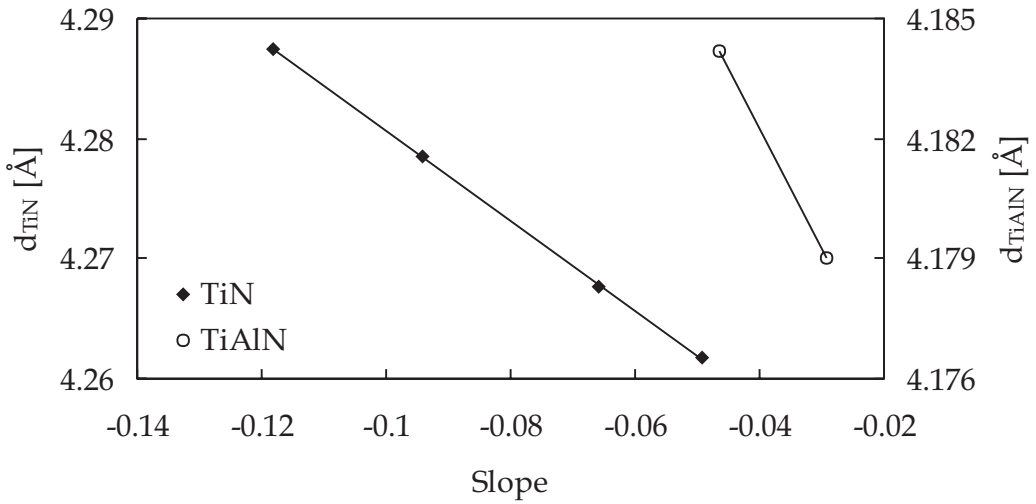

Figure 5.9 Determining the Poisson's ratios by plotting the intercept of the d-sin$^2\psi$ graph as a function of the slope.

The d_0 of TiN is just a little larger than the value of stoichiometric TiN from literature, which is 4.2417 Å. With the unstrained lattice spacing of TiAlN, 4.170 Å, it is possible to calculate the composition assuming that Vegard's law is applicable [9]. It results in a chemical composition of $Ti_{0.41\pm0.04}Al_{0.59\pm0.04}N$.

Table 5.4 Calculated Poisson's ratios of TiN and TiAlN

System	TiN	TiAlN
d_0 [Å]	4.2430 ± 0.001	4.170 ± 0.005
$Sin^2\psi$	0.376 ± 0.003	0.301 ± 0.005
ν	0.232 ± 0.002	0.177 ± 0.003

The macro residual stresses can now be calculated, see Table 5.5. The residual stresses in the coatings deposited on stainless steel are for all systems higher than the residual stresses in the coatings deposited on tool steel. Furthermore, the residual stress in the TiN sub-layers is much higher than the stress in the TiAlN sub-layers and is also higher than the stress in the single TiN films.

Table 5.5 Calculated residual stresses [GPa], E=450 GPa and ν_{TiN}=0.232 and ν_{TiAlN}=0.177.

Substrate		Stainless steel	Tool steel
TiN film		-5.6 ± 0.1	-4.2 ± 0.2
Multi-layer	TiN	-10.1 ± 0.3	-8.0 ± 0.4
	TiAlN	-4.2 ± 0.2	-2.7 ± 0.1

The difference between the stainless steel and the tool steel may be explained by looking at the expansion coefficients of the substrates, stainless steel ≈(17.8 – 18.4)·10^{-6} [K^{-1}] and tool steel ≈(11.9 – 12.9)·10^{-6} [K^{-1}] [2,13,14,15]. Therefore, the thermal stress is higher for the layers on stainless steel than for the ones on tool steel and the thermal stress in the TiN will be of the same magnitude as in the TiAlN. The difference between the residual stress in TiN and TiAlN is a consequence of the atomic peening [16], which is apparently present for TiN [17] and absent or very small for the TiAlN sub-layers.

Part of the difference between the stress in the TiN sub-layers and the TiN films may be a result of the difference in layer thickness. The residual stress in a PVD layer decreases as the layer thickness increases [17]. Hence, it is expected that the macro residual stress in the TiN sub-layers with a thickness of 20 nm, are higher than in the 4 μm TiN films.

Conclusions

Investigation of PVD films of alternating TiN and TiAlN layers and single TiN films shows that the multi-layers are only slightly textured and that they have a {311} texture. The residual stresses in the TiN and TiAlN sub-layers of the multi-layer systems show a large difference. The compressive stresses in the TiN are 8 to 10 GPa and the compressive stresses in the TiAlN are only 3 to 4 GPa. The difference is a result of the stress due to the atomic peening. The later is not present or very small for the TiAlN. The main difference between the layers on the two substrates is a consequence of the difference in linear expansion. With this difference it is possible to determine Poisson's ratio for TiAlN, which is 0.177.

References

1 K.N. Anders, J.E. Bienk, K.O. Schweitz, H. Reitz, J. Chevallier, P. Kringhoj, J. Bottiger, Surf. Coat. Technol. 123 (2000) 219.
2 D. Y. Wang, C.L. Chang, K.W. Wong, Y. W. Li, Y. Ho, Surf. Coat. Technol. 120/121 (1999) 388.
3 K.H. Kim, S.H. Lee, Thin Solid Films 283 (1996) 165.
4 J.R. Roos, J.P. Celis, E. Vancoille, H. Veltrop, S. Boelens, F. Jungblut, J. Ebberink, H. Homberg, Thin Solid Films 193/194 (1990) 547.
5 J.E. Sundgren, A. Rockett, J.E. Greene, U Helmersson, J. Vac. Sci. Technol. A4(6) (1986) 2770.
6 A. Kimura, H. Hasegawa, K. Yamada, T. Suzuki, Surf. Coat. Technol. 120/121 (1999) 438.
7 B.D. Cullity, Elements of X-Ray Diffraction, Addison-Wesley Inc., Reading, Massachusetts, 1978.
8 G. Hakansson, J.E. Sundgren, D. McIntyre, J.E. Greene, W.D. Münz, Thin Solid Films 153 (1987) 55.
9 U. Wahlström, L. Hultman, J.E. Sundgren, F. Adibi, I. Petrov, J.E. Greene, Thin Solid Films 235 (1993) 62.
10 I.C. Noyan, J.B. Cohen, Residual stress, Springer-Verlag Inc., New York, 1987.
11 D.J.H. Teeuw, J.Th.M. De Hosson, J. Mat. Research 13 (1998) 1757.
12 J.A. Sue, Surf. Coat. Technol. 54/55 (1992) 154.
13 G. Dreier, S. Schmauder, Scripta Metall. Mater. 28 (1993) 103.
14 Metals handbook, Vol 3, 9th ed., American Society For Metals, Ohio, USA, 1980 p. 441.
15 Y.S. Touloukian, R.K. Kirby, R.E. Taylor, T.Y.R. Lee, Thermophysical Properties of Matter, Nonmetallic Solids, Vol 13, IFI/Plenum, 1977, p1322.
16 C.A. Davis, Thin Solid Films 226 (1992) 30.
17 J.-D. Kamminga, Th.H. de Keijser, R. Delhez, E.J. Mittemeijer, Thin Solid Films 317 (1998) 169.